ACS central science

http://pubs.acs.org/journal/acscii

Research Article

Hydrazine-Hydrazide-Linked Covalent Organic Frameworks for Water Harvesting

Ha L. Nguyen,[⊥] Cornelius Gropp,[⊥] Nikita Hanikel, Anna Möckel, Alicia Lund, and Omar M. Yaghi*

Cite This: *ACS Cent. Sci.* 2022, 8, 926–932

Read Online

ACCESS | Metrics & More | Article Recommendations | Supporting Information

ABSTRACT: We report a postsynthetic strategy and its implementation to make covalent organic frameworks (COFs) with irreversible hydrazide linkages. This involved the synthesis of three 2D and 3D hydrazine-linked frameworks and their partial oxidation. The linkage synthesis and functional group transformation—hydrazine and hydrazide—were evidenced by ^{15}N multi-CP-MAS NMR. In addition, the isothermal water uptake profiles of these frameworks were studied, leading to the discovery of one hydrazine-hydrazide-linked COF suitable for water harvesting from air in arid conditions. This COF displayed characteristic S-shaped water sorption profiles, a steep pore-filling step below 18% relative humidity at 25 °C, and a total uptake capacity of 0.45 g g^{-1}. We found that even small changes made on the molecular level can lead to major differences in the water isotherm profiles, therefore pointing to the utility of water sorption analysis as a complementary analytical tool to study linkage transformations.

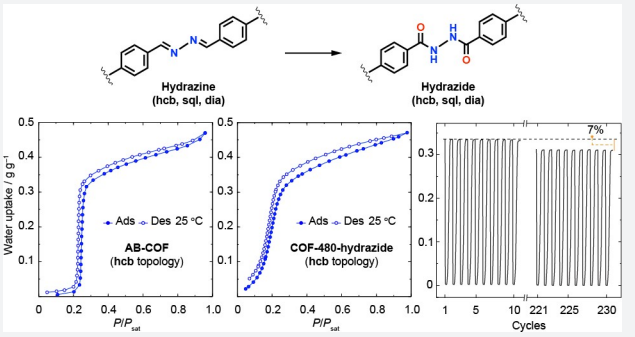

INTRODUCTION

Multistep organic synthetic methods have been successfully translated to the solid state.[1−4] This practice has become especially attractive for the synthesis of new covalent organic frameworks (COFs).[5−8] Their hallmark features, porosity and crystallinity, allow chemical transformations to be done on the framework and enable rigorous analysis of concurrent structural changes through diffraction and spectroscopic techniques.[5,6]

The synthesis of COFs relies on an initial reversible step to guide the covalent assembly of organic building units into extended and crystalline structures.[9−12] This step can be followed by one or more postsynthetic transformations, leading to structural complexity and function of the framework.[5,8,10,11] This has been demonstrated for a number of imine-linked COFs,[13−15] but hydrazide moieties have not been reported yet.

Here, we report three 2D and 3D hydrazide-linked COFs following postsynthetic oxidation of the hydrazine-linking units (Scheme 1). Considering the rather hydrophilic nature of the hydrazine and hydrazide linkages, we chose to study the effect of the synthetic transformations with water vapor sorption analysis.[16,17] This not only allowed us to explore new sorbents for water harvesting from air but also provided us with additional insight into the micro- and macroscopic changes occurring on the framework.

Our synthetic strategy toward hydrazide-linked COFs is based on the reversible formation of the hydrazine-linkage, followed by postsynthetic oxidation to the hydrazide (Scheme 1). We first demonstrated the feasibility of this route on a molecular model system. Then, we explored its transferability to the solid state by synthesizing two 2D COFs with honeycomb (**hcb**) and square-lattice (**sql**) topologies and one 3D COF with diamond (**dia**) topology. In total, six COFs were synthesized, four of which were hitherto unreported, and comprised of hydrazine and hydrazide linkages—the latter presents a linkage that has not been reported in COF chemistry yet. The COFs were analyzed by ^{15}N multiple cross-polarization magic-angle spinning spectroscopy (multi-CP-MAS NMR),[18] giving a quantitative readout of the chemical transformations. Fourier-transform infrared (FT-IR), solid-

Scheme 1. Synthetic Strategy for Hydrazide-Linked COFs[a]

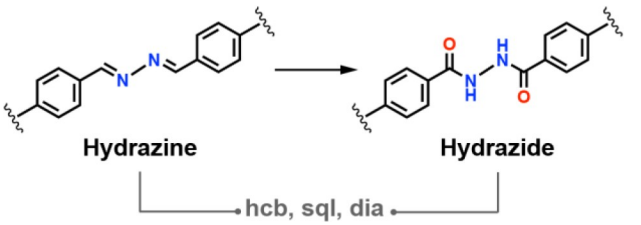

[a]This strategy was applied to a molecular model system and two 2D (hcb, sql) and one 3D (dia) COFs.

Received: April 4, 2022
Published: June 16, 2022

https://doi.org/10.1021/acscentsci.2c00398
ACS Cent. Sci. 2022, 8, 926−932

Scheme 2. Overview of the Synthesis of (a) 2D hcb, (b) 2D sql, and (c) 3D dia Hydrazide-Linked COFs[a]

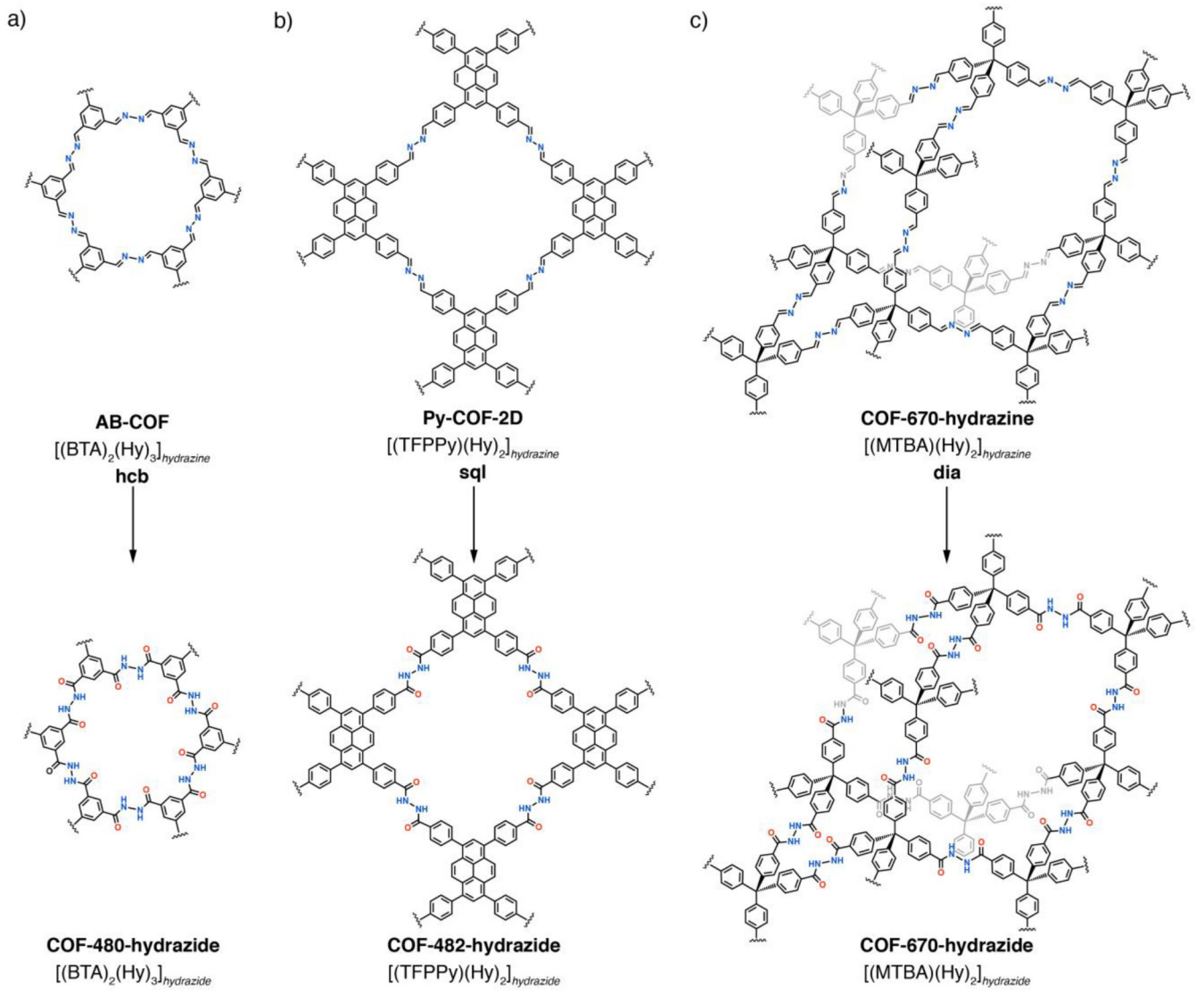

[a]The synthesis of hydrazine-linked COFs is detailed in the Supporting Information.

and solution-state nuclear magnetic resonance (NMR) spectroscopies, elemental analysis (EA), thermogravimetric analysis (TGA), powder X-ray diffraction (PXRD), and nitrogen sorption substantiated the structural and compositional integrity of the frameworks.

RESULTS AND DISCUSSION

To show the viability of our postsynthetic strategy, we first synthesized a hydrazine molecular model compound, 1,2-benzylidenehydrazine, from benzaldehyde and hydrazine with quantitative yield (Scheme 1).[19] The hydrazine compound was subsequently oxidized to afford the hydrazide molecular model using previously reported conditions for the conversion of imines to amides in COFs (see Supporting Information, section S2).[5]

To demonstrate the transferability from solution to the solid state, we first synthesized two 2D and one 3D hydrazine-linked COFs (Scheme 2). AB-COF[20,21] was produced from trigonal-planar 1,3,5-benzenetrialdehyde (BTA) and linear hydrazine (Hy), and crystallized in the **hcb** topology with the reticular formula $[(BTA)_2(Hy)_3]_{hydrazine}$. Py-COF-2D[22] is comprised of the square-planar 1,3,6,8-tetrakis(*p*-formylphenyl)pyrene (TFPPy) unit and Hy and crystallized in the **sql** topology with the reticular formula $[(TFPPy)(Hy)_2]_{hydrazine}$. Lastly, COF-670-hydrazine was synthesized from the tetrahedral 4,4′,4″,4‴-methanetetrayltetrabenzaldehyde (MTBA) and Hy and crystallized in the **dia** topology with the reticular formula $[(MTBA)(Hy)_2]_{hydrazine}$ (Scheme 2). While AB-COF and Py-COF-2D have been previously reported,[20,21] a hydrazine-linked 3D COF, COF-670-hydrazine, has not been reported to date.

We first explored the oxidation of the hydrazine-linked AB-COF by subjecting it to our reported oxidation conditions[5] involving the use of $NaClO_2$ as oxidant in an aqueous acidic medium in the presence of 2-methyl-2-butene over 3 days to obtain COF-480-hydrazide (see Supporting Information, section S2). FT-IR spectroscopic traces of the product indicated attenuation of the imine band at 1625 cm^{-1} corresponding to the hydrazine linkages and an emerging band at 1674 cm^{-1}, which was assigned to the carbonyl stretching vibration of the hydrazide moiety (see Supporting Information, section S3). The solid-state ^{15}N multi-CP-MAS

https://doi.org/10.1021/acscentsci.2c00398
ACS Cent. Sci. 2022, 8, 926−932

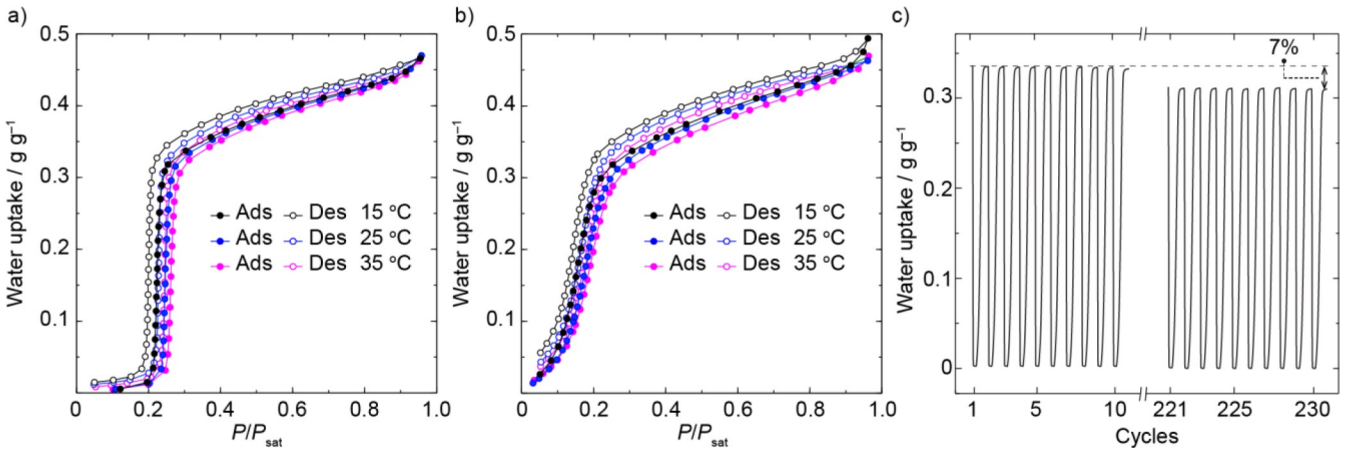

Figure 1. Water vapor sorption analysis of AB-COF (a) and COF-480-hydrazide (b) at different temperatures (15, 25, and 35 °C). *P*: water vapor pressure. P_{sat}: saturation water vapor pressure at the given temperature. Water cycling stability test of 230 adsorption−desorption cycles of COF-480-hydrazide (c) subjected to an isobaric (1.7 kPa water vapor) temperature-swing adsorption between 30 and 85 °C, corresponding to 40% and 3% RH, respectively. The full data set is reported in the Supporting Information, section S8.

NMR spectroscopy,[18] performed on a 50% ^{15}N-labeled sample, further corroborated the transformation with a new peak at 171.7 ppm. However, no quantitative conversion was observed, despite prolonged reaction times or an increased amount of oxidation reagent (see Supporting Information, section S2). This led us to the conclusion that only partial oxidation was achieved—an observation that we further substantiated with an ^{15}N NMR experiment on the hydrazide model system (see Supporting Information, section S4). Multi-CP-MAS NMR on the ^{15}N-labeled COF samples allowed us to quantify the conversion, which amounted to 9.2% (see Supporting Information, section S4). Here, the resonances corresponding to the functionalities were fit to Gaussian line shapes, and their relative areas were compared. This analysis correlated well with the atomic composition determined by EA (see Supporting Information, section S2). TGA under nitrogen and air flow revealed an onset in decomposition for the pristine and the oxidized samples at around 380 °C.

PXRD analysis of the microcrystalline powder confirmed retention of crystallinity after oxidation and did not reveal additional diffraction peaks associated with hydrolyzed starting materials or additives (see Supporting Information, section S6). The PXRD pattern of AB-COF shows high-intensity peaks at 6.8°, 11.8°, and 26.4° 2θ values, associated with the (100), (1$\bar{2}$0), and (002) lattice planes. After oxidation, the broad peak indexed as the lattice plane (002) shifted to a higher 2θ value (26.6°), resulting from changes in the interlayer stacking of the structure.

N_2 sorption analysis at 77 K of the pristine AB-COF and COF-480-hydrazide demonstrated permanent porosity and revealed a Type I isotherm, indicating a micropore structure. The Brunauer−Emmett−Teller (BET) surface areas were calculated to be 1209 and 989 m^2 g^{-1}, respectively. The pore size distribution, estimated from the N_2 isotherms and calculated by density functional theory (DFT) using the cylinder geometry, indicated comparable pore sizes of around 11 Å in diameter (see Supporting Information, section S7).

To gain further insight into the impact of the chemical transformations on the water sorption behavior, we measured the water sorption isotherms at 15, 25, and 35 °C (Figure 1a,b). AB-COF displays an S-shaped water sorption isotherm with a steep pore-filling step at around 23% relative humidity (RH) at 25 °C (Figure 1a). The maximal uptake at P/P_{sat} = 0.95 reaches a total uptake capacity of 0.45 g g^{-1}. After oxidation, the water sorption isotherm of COF-480-hydrazide substantially shifts to lower RH with a steep pore-filling step at 18%—thus extending the RH range at which COF-480-hydrazide can operate to more arid conditions. Importantly, the COF preserves its total water uptake capacity of around 0.45 g g^{-1} at P/P_{sat} = 0.95 (25 °C).

Furthermore, the water sorption isotherm profiles are retained at 15 and 35 °C, indicating robust sorption behavior under varying temperatures. The increased water uptake capacity at lower RH upon oxidation indicated stronger water−framework interactions during the pore-filling step.[23,24] To evaluate the strength of these interactions, the isosteric heat of water adsorption (Q_{st}) was calculated with the Clausius−Clapeyron equation using the water isotherms at 15, 25, and 35 °C. The Q_{st} was estimated to be 49 kJ mol^{-1} for the pristine AB-COF and 50.5 kJ mol^{-1} for the oxidized COF-480-hydrazide. A ΔQ_{st} = 1.5 kJ mol^{-1} upon oxidation likely results from the stronger hydrogen-bonding donor and acceptor sites in the framework, given that both COFs show comparable pore diameters of around 11 Å.

It is noteworthy that even such a small conversion (9.2%) significantly shifted the water uptake to lower RH and resulted in an increase in water affinity to the framework. Thus, COF-480-hydrazide extracts water from air at even lower humidity compared to the pristine hydrazine-linked COF, AB-COF.[21]

To test the long-term stability of COF-480-hydrazide over multiple water adsorption−desorption cycles, we subjected the COF to an isobaric (1.7 kPa water vapor) temperature-swing adsorption between 30 and 85 °C, corresponding to 40% and 3% RH, respectively. The water uptake working capacity under these conditions was 0.33 g g^{-1}. After 230 adsorption−desorption cycles, we observed a reduction of the working capacity by 7% (Figure 1c). This is attributed to partial hydrolysis of the sample upon long-term exposure to water vapor at an elevated temperature.

Next, we pursued the oxidation of the hydrazine-linked Py-COF-2D to COF-482-hydrazide. Noteworthy, partial oxidation of the hydrazine to the hydrazide linkage was already observed during the synthesis of the Py-COF-2D— even under inert reaction conditions (N_2 atmosphere; see Supporting Informa-

https://doi.org/10.1021/acscentsci.2c00398
ACS Cent. Sci. 2022, 8, 926−932

tion, section S2). This phenomenon was mentioned by Lotsch and co-workers,[25] and in our work, the observation was substantiated by FT-IR spectroscopy and ^{15}N multi-CP-MAS NMR spectroscopy on a 50% ^{15}N-labeled sample (see Supporting Information, sections S3 and S4). Presumably, both steric and electronic effects contribute to the more facile oxidation of Py-COF-2D as compared to AB-COF.

For further oxidation, we applied comparable conditions as described for AB-COF. Similarly, we observed enhanced attenuation of the characteristic imine band at 1625 cm^{-1} in the FT-IR spectroscopic traces and a relative increase of the carbonyl band at 1674 cm^{-1}. The solid-state ^{15}N multi-CP-MAS NMR spectroscopy on a 50% ^{15}N-labeled sample showed an enhanced peak at 125.3 ppm, further substantiating successful oxidation. The conversion of the hydrazine- to the hydrazide-linkage amounted to 26.3% conversion (see Supporting Information, section S4). TGA under nitrogen and air flow revealed a comparable onset in decomposition for the pristine and oxidized samples at around 500 °C.

PXRD analysis of the microcrystalline powder of Py-COF-2D and COF-482-hydrazide indicated retention of crystallinity after oxidation (see Supporting Information, section S6). Furthermore, the PXRD traces indicated a shift of the highest intensity peaks from 4.5° 2θ, associated with the (1$\bar{1}$0) lattice plane, for the hydrazine-linked COF to 4.6° 2θ for the hydrazide COF. This observation correlates well with the anticipated changes in unit cell parameters upon oxidation (see Supporting Information, section S6).

N_2 sorption analysis at 77 K of Py-COF-2D and COF-482-hydrazide demonstrated permanent porosity and revealed a Type I isotherm, indicating a micropore structure. The calculated BET surface areas amounted to 1850 m^2 g^{-1} for the hydrazine-linked Py-COF-2D and 1700 m^2 g^{-1} for COF-482-hydrazide. The reduction in specific surface area is in line with the weight increase upon oxidation. The pore size distribution, calculated from the N_2 adsorption isotherms using the above-described parameters, indicated two kinds of pores with diameters of 15.9 and 18.5 Å for Py-COF-2D and 15.4 and 18.5 Å for the oxidized COF-482-hydrazide.

The pristine Py-COF-2D displayed an S-shaped water sorption isotherm with a steep pore-filling step at around 52% RH and a total uptake 0.75 g g^{-1} at 25 °C (Figure 2). Upon oxidation, the isotherm profile significantly shifted to 42% RH with a slightly lower total uptake of 0.70 g g^{-1} at 25 °C. The shift of the pore-filling step to lower RH upon oxidation is in line with our previous observation in AB-COF and presumably stems from the incorporation of the more polar hydrazide functionalities into the framework.

This is one of the first examples where postsynthetic transformations on COFs enabled a shift of the pore-filling step of the water isotherms to lower RH.[26,27] The difference in the Q_{st} between the pristine Py-COF-2D and COF-482-hydrazide, calculated from the water sorption isotherms at 15, 25, and 35 °C, amounted to ΔQ_{st} = 2 kJ mol^{-1} (Q_{st} = 45 and 47 kJ mol^{-1}, respectively). A comparable ΔQ_{st} of the pristine sample and the oxidized hydrazide sample was also observed for AB-COF and COF-480-hydrazide.

Finally, to demonstrate postsynthetic oxidation of hydrazine- to hydrazide-linked COFs in 3D, we synthesized COF-670-hydrazine from the tetrahedral MTBA and linear hydrazine building units (Scheme 1c and Figure 3a). The structure crystallized in the **dia** topology with six-fold interpenetration (see Supporting Information, section S6). Similar to our

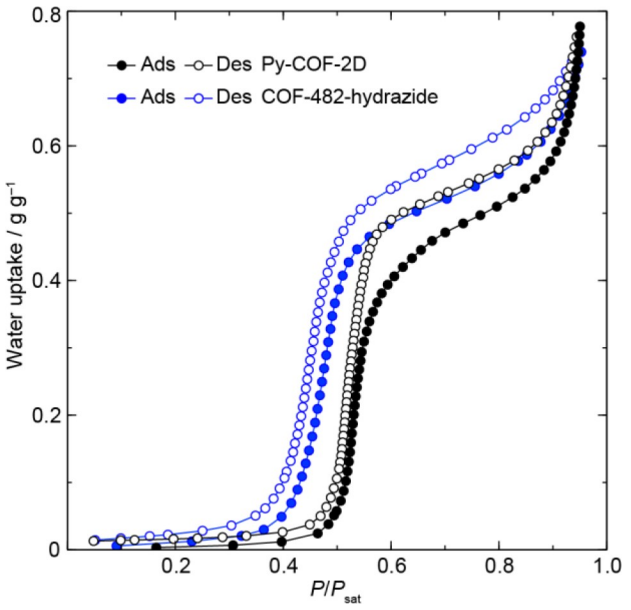

Figure 2. Overlay of water isotherms of Py-COF-2D and COF-482-hydrazide at 25 °C. P: water vapor pressure. P_{sat}: saturation water vapor pressure.

observation with Py-COF-2D, partial oxidation of the hydrazine to hydrazide units in COF-670-hydrazine was already observed at this stage (see FT-IR and ^{15}N spectroscopic traces, sections S3 and S4 in the Supporting Information). This confirmed the susceptibility of the 3D COF to oxidation. Upon further oxidation, we observed enhanced attenuation of the characteristic imine band at 1625 cm^{-1} in the FT-IR spectroscopic traces and a more intensive band at 1674 cm^{-1} (see Supporting Information, section S3). Successful oxidation was further confirmed through ^{15}N solid-state CP-MAS NMR spectroscopy on a 50% ^{15}N-labeled sample before and after oxidation. The ^{15}N NMR peaks at 127.8 ppm intensified upon oxidation, and the conversion of the hydrazine- to the hydrazide-linkage amounted to 13.4% (Figure 3b and Supporting Information, section S4). TGA under nitrogen and air flow revealed an increase in thermal stability upon oxidation of the hydrazine-linked COF. Here, COF-670-hydrazine and COF-670-hydrazide showed an onset in thermal decomposition at around 350 °C.

PXRD analysis of the microcrystalline powder of the hydrazine-linked COF and comparison with structural models of varying degrees of interpenetration allowed us to assign the degree of interpenetration to six-fold (Figure 3c). After oxidation, PXRD indicated retention of the crystallinity (Figure 3d and Supporting Information, section S6). Furthermore, the PXRD traces indicated a small shift of the highest intensity peaks at 9.4° 2θ, associated with the (020) lattice plane, for the hydrazine-linked COF to 9.5° 2θ for the hydrazide-linked COF. This observation correlated well with the anticipated changes in unit cell parameters upon oxidation (see Supporting Information, section S6). We also observed shifts to higher 2θ values for the designated reflections occurring between 13° and 25°.

N_2 sorption analysis at 77 K of the two samples demonstrated permanent porosity and revealed a Type I isotherm, indicating a micropore structure. The calculated BET surface areas amounted to 1209 m^2 g^{-1} for the hydrazine-linked COF-670-hydrazine and 699 m^2 g^{-1} for COF-670-

https://doi.org/10.1021/acscentsci.2c00398
ACS Cent. Sci. 2022, 8, 926−932

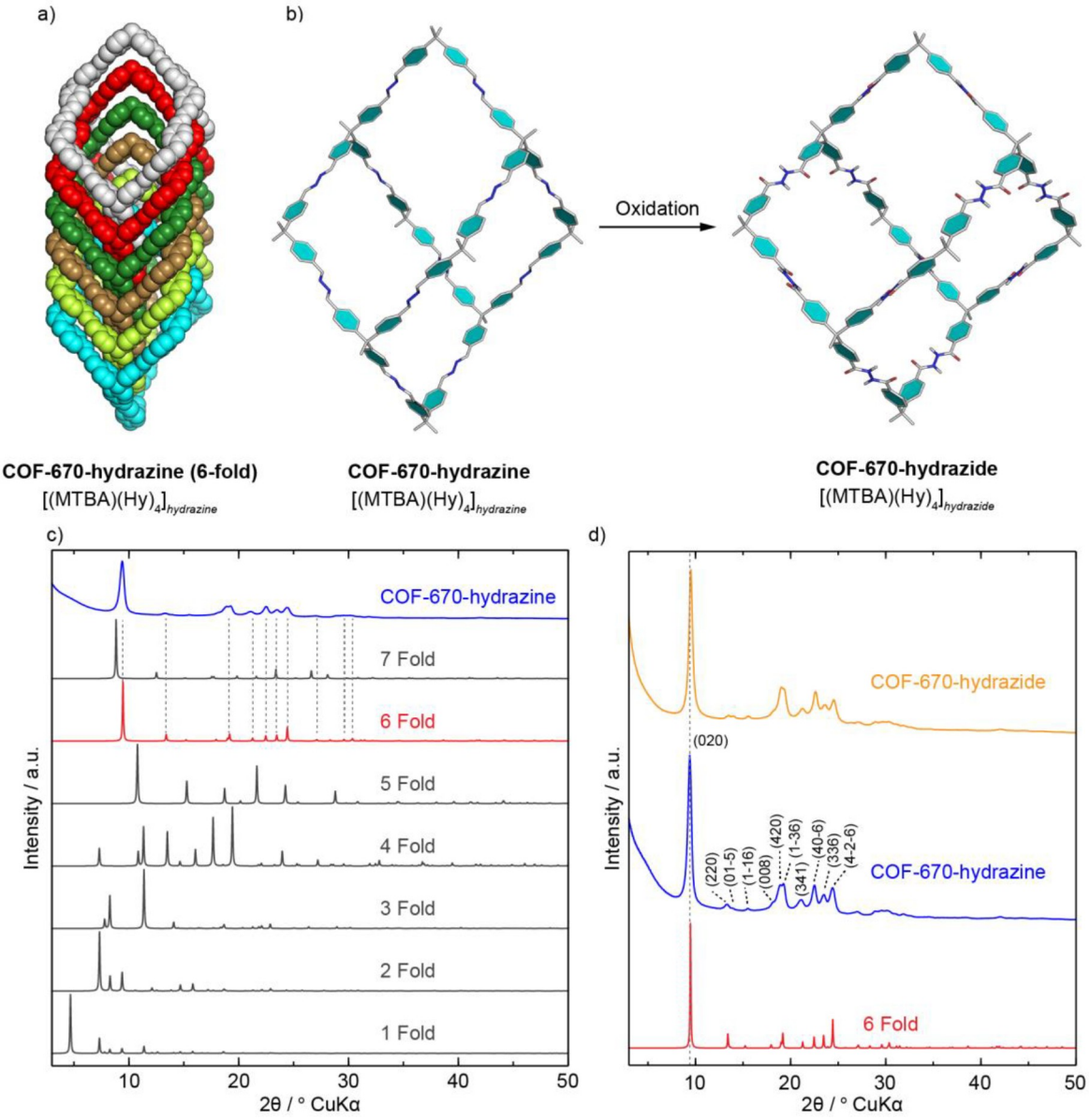

Figure 3. Structural models of the six-fold framework of COF-670-hydrazine (a) and the oxidation of COF-670-hydrazine to COF-670-hydrazide (b). Overlay of PXRD patterns of COF-670-hydrazine modeled structures (from one-fold to seven-fold) and its experimental PXRD pattern (c). PXRD patterns of simulated COF-670-hydrazine compared to the experimental ones of COF-670-hydrazine and COF-670-hydrazide (d).

hydrazide. The pore size distributions, calculated from the N_2 adsorption isotherms using the above-described parameters, indicated overall retention of the pore diameters of 6 Å after the oxidation (see Supporting Information, section S7).

The pristine COF-670-hydrazine displayed a water sorption isotherm with a slightly sloped pore-filling step at around 43% RH and a total uptake of 0.33 g g^{-1} at 25 °C (see Supporting Information, section S8).

CONCLUSION

We synthesized a series of 2D and 3D hydrazine-hydrazide-linked COFs by applying a postsynthetic strategy. This involved first the synthesis of the hydrazine-linked frameworks, followed by oxidation to afford the hydrazine-hydrazide-linked structures, in which the synthesis and partial transformation from hydrazine to hydrazide were further substantiated by ^{15}N multi-CP-MAS NMR. In addition, we subjected the frameworks to isothermal water sorption analysis. This not only allowed us to discover new structures capable of water harvesting from desert air but also provided us with additional insight into the micro- and macroscopic changes occurring in the framework. Importantly, we found that even small modifications of the molecular structures of the frameworks can lead to impactful differences in the water isotherm profiles. Overall, this study expands the scope of COF chemistry to include crystallization of irreversible linkages and shows that these new systems can extract water from low-humidity air.

ASSOCIATED CONTENT

Supporting Information

The Supporting Information is available free of charge at https://pubs.acs.org/doi/10.1021/acscentsci.2c00398.

Synthesis and full characterization of COFs including EA, FT-IR spectroscopy, NMR spectra, PXRD data,

https://doi.org/10.1021/acscentsci.2c00398
ACS Cent. Sci. 2022, 8, 926−932

computational modeling, gas uptake measurements, TGA, and water isotherms (PDF)

Crystallographic information file (CIF) of COF-670-hydrazine (model structure of the six-fold framework) (CIF)

Accession Codes

CCDC 2164351 contains the supplementary crystallographic data for COF-670-hydrazine. These data can be obtained free of charge via www.ccdc.cam.ac.uk/data_request/cif, or by emailing data_request@ccdc.cam.ac.uk, or by contacting The Cambridge Crystallographic Data Centre, 12 Union Road, Cambridge CB2 1EZ, UK; fax: + 44 1223 336033.

AUTHOR INFORMATION

Corresponding Author

Omar M. Yaghi − *Department of Chemistry, University of California−Berkeley, Kavli Energy Nanoscience Institute at UC Berkeley; and Berkeley Global Science Institute, Berkeley, California 94720, United States; Joint UAEU−UC Berkeley Laboratories for Materials Innovations, United Arab Emirates University, Al-Ain 15551, United Arab Emirates;* orcid.org/0000-0002-5611-3325; Email: yaghi@berkeley.edu

Authors

Ha L. Nguyen − *Department of Chemistry, University of California−Berkeley, Kavli Energy Nanoscience Institute at UC Berkeley; and Berkeley Global Science Institute, Berkeley, California 94720, United States; Joint UAEU−UC Berkeley Laboratories for Materials Innovations, United Arab Emirates University, Al-Ain 15551, United Arab Emirates;* orcid.org/0000-0002-4977-925X

Cornelius Gropp − *Department of Chemistry, University of California−Berkeley, Kavli Energy Nanoscience Institute at UC Berkeley; and Berkeley Global Science Institute, Berkeley, California 94720, United States*

Nikita Hanikel − *Department of Chemistry, University of California−Berkeley, Kavli Energy Nanoscience Institute at UC Berkeley; and Berkeley Global Science Institute, Berkeley, California 94720, United States;* orcid.org/0000-0002-3292-5070

Anna Möckel − *Department of Chemistry, University of California−Berkeley, Kavli Energy Nanoscience Institute at UC Berkeley; and Berkeley Global Science Institute, Berkeley, California 94720, United States*

Alicia Lund − *Department of Chemistry, University of California−Berkeley, Berkeley, California 94720, United States;* orcid.org/0000-0001-7520-9544

Complete contact information is available at: https://pubs.acs.org/10.1021/acscentsci.2c00398

Author Contributions

[⊥]H.L.N. and C.G. contributed equally. H.L.N. and C.G. conceived the idea. H.L.N., C.G., and A.M. synthesized and characterized materials. N.H. and A.L. collected and interpreted data on water vapor sorption and quantitative ^{15}N NMR spectra, respectively. O.M.Y. directed the project. The manuscript was written through contributions of all authors.

Notes

The authors declare the following competing financial interest(s): Omar M. Yaghi is co-founder of Water HarvestingInc., aiming at commercializing related technologies.

ACKNOWLEDGMENTS

We acknowledge the financial support from the Defense Advanced Research Projects Agency (DARPA) under Contract No: HR0011-21-C-0020. Any opinions, findings and conclusions or recommendations expressed in this material are those of the author(s) and do not necessarily reflect the views of the DARPA. C.G. is a Leopoldina postdoctoral fellow of the German National Academy of Science (LPDS 2019-02). N.H. thanks the Studienstiftung des deutschen Volkes and acknowledges the receipt of the Kavli ENSI Philomathia Graduate Student Fellowship and Blavatnik Innovation Fellowship. We acknowledge the College of Chemistry Nuclear Magnetic Resonance Facility for resources and staff assistance, where instruments are partially supported by NIH S10OD024998. We thank Ms. Carlijn van Beek for synthetic contributions.

ABBREVIATIONS

COFs, covalent organic frameworks; EA, elemental analysis; FT-IR, Fourier-transform infrared spectroscopy; NMR, nuclear magnetic resonance spectroscopy; PXRD, powder X-ray diffraction; TGA, thermogravimetric analysis

REFERENCES

(1) Hawker, C. J.; Wooley, K. L. The Convergence of Synthetic Organic and Polymer Chemistries. *Science* **2005**, *309*, 1200−1205.

(2) Fracaroli, A. M.; Siman, P.; Nagib, D. A.; Suzuki, M.; Furukawa, H.; Toste, F. D.; Yaghi, O. M. Seven Post-Synthetic Covalent Reactions in Tandem Leading to Enzyme-like Complexity within Metal−Organic Framework Crystals. *J. Am. Chem. Soc.* **2016**, *138*, 8352−8355.

(3) Yaghi, O. M.; Kalmutzki, M. J.; Diercks, C. S. *Introduction to Reticular Chemistry: Metal-Organic Frameworks and Covalent Organic Frameworks*; Wiley-VCH: Weinheim, 2019.

(4) Kalaj, M.; Cohen, S. M. Postsynthetic Modification: An Enabling Technology for the Advancement of Metal−Organic Frameworks. *ACS Cent. Sci.* **2020**, *6*, 1046−1057.

(5) Waller, P. J.; Lyle, S. J.; Osborn Popp, T. M.; Diercks, C. S.; Reimer, J. A.; Yaghi, O. M. Chemical Conversion of Linkages in Covalent Organic Frameworks. *J. Am. Chem. Soc.* **2016**, *138*, 15519−15522.

(6) Lyle, S. J.; Osborn Popp, T. M.; Waller, P. J.; Pei, X.; Reimer, J. A.; Yaghi, O. M. Multistep Solid-State Organic Synthesis of Carbamate-Linked Covalent Organic Frameworks. *J. Am. Chem. Soc.* **2019**, *141*, 11253−11258.

(7) Lyle, S. J.; Waller, P. J.; Yaghi, O. M. Covalent Organic Frameworks: Organic Chemistry Extended into Two and Three Dimensions. *Trends Chem.* **2019**, *1*, 172−184.

(8) Segura, J. L.; Royuela, S.; Mar Ramos, M. Post-Synthetic Modification of Covalent Organic Frameworks. *Chem. Soc. Rev.* **2019**, *48*, 3903−3945.

(9) Diercks, C. S.; Yaghi, O. M. The Atom, the Molecule, and the Covalent Organic Framework. *Science* **2017**, *355*, eaal1585.

(10) Lohse, M. S.; Bein, T. Covalent Organic Frameworks: Structures, Synthesis, and Applications. *Adv. Funct. Mater.* **2018**, *28*, 1705553.

(11) Geng, K.; He, T.; Liu, R.; Dalapati, S.; Tan, K. T.; Li, Z.; Tao, S.; Gong, Y.; Jiang, Q.; Jiang, D. Covalent Organic Frameworks: Design, Synthesis, and Functions. *Chem. Rev.* **2020**, *120*, 8814−8933.

(12) Haase, F.; Lotsch, B. V. Solving the COF Trilemma: Towards Crystalline, Stable and Functional Covalent Organic Frameworks. *Chem. Soc. Rev.* **2020**, *49*, 8469−8500.

(13) Haase, F.; Troschke, E.; Savasci, G.; Banerjee, T.; Duppel, V.; Dörfler, S.; Grundei, M. M. J.; Burow, A. M.; Ochsenfeld, C.; Kaskel, S.; Lotsch, B. V. Topochemical Conversion of an Imine- into a Thiazole-Linked Covalent Organic Framework Enabling Real Structure Analysis. *Nat. Commun.* **2018**, *9*, 2600.
(14) Waller, P. J.; Alfaraj, Y. S.; Diercks, C. S.; Jarenwattananon, N. N.; Yaghi, O. M. Conversion of Imine to Oxazole and Thiazole Linkages in Covalent Organic Frameworks. *J. Am. Chem. Soc.* **2018**, *140*, 9099−9103.
(15) Cusin, L.; Peng, H.; Ciesielski, A.; Samorì, P. Chemical Conversion and Locking of the Imine Linkage: Enhancing the Functionality of Covalent Organic Frameworks. *Angew. Chemie Int. Ed.* **2021**, *60*, 14236−14250.
(16) Fathieh, F.; Kalmutzki, M. J.; Kapustin, E. A.; Waller, P. J.; Yang, J.; Yaghi, O. M. Practical Water Production from Desert Air. *Sci. Adv.* **2018**, *4*, eaat3198.
(17) Hanikel, N.; Pei, X.; Chheda, S.; Lyu, H.; Jeong, W.; Sauer, J.; Gagliardi, L.; Yaghi, O. M. Evolution of Water Structures in Metal-Organic Frameworks for Improved Atmospheric Water Harvesting. *Science* **2021**, *374*, 454−459.
(18) Massiot, D.; Fayon, F.; Capron, M.; King, I.; Le Calvé, S.; Alonso, B.; Durand, J.-O.; Bujoli, B.; Gan, Z.; Hoatson, G. Modelling One- and Two-Dimensional Solid-State NMR Spectra. *Magn. Reson. Chem.* **2002**, *40*, 70−76.
(19) Sek, D.; Siwy, M.; Bijak, K.; Grucela-Zajac, M.; Malecki, G.; Smolarek, K.; Bujak, L.; Mackowski, S.; Schab-Balcerzak, E. Comparative Studies of Structural, Thermal, Optical, and Electrochemical Properties of Azines with Different End Groups with Their Azomethine Analogues toward Application in (Opto)Electronics. *J. Phys. Chem. A* **2013**, *117*, 10320−10332.
(20) Li, Z.; Feng, X.; Zou, Y.; Zhang, Y.; Xia, H.; Liu, X.; Mu, Y. A 2D Azine-Linked Covalent Organic Framework for Gas Storage Applications. *Chem. Commun.* **2014**, *50*, 13825−13828.
(21) Stegbauer, L.; Hahn, M. W.; Jentys, A.; Savasci, G.; Ochsenfeld, C.; Lercher, J. A.; Lotsch, B. V. Tunable Water and CO2 Sorption Properties in Isostructural Azine-Based Covalent Organic Frameworks through Polarity Engineering. *Chem. Mater.* **2015**, *27*, 7874−7881.
(22) Dalapati, S.; Jin, S.; Gao, J.; Xu, Y.; Nagai, A.; Jiang, D. An Azine-Linked Covalent Organic Framework. *J. Am. Chem. Soc.* **2013**, *135*, 17310−17313.
(23) Furukawa, H.; Gándara, F.; Zhang, Y. B.; Jiang, J.; Queen, W. L.; Hudson, M. R.; Yaghi, O. M. Water Adsorption in Porous Metal-Organic Frameworks and Related Materials. *J. Am. Chem. Soc.* **2014**, *136*, 4369−4381.
(24) Nguyen, H. L.; Hanikel, N.; Lyle, S. J.; Zhu, C.; Proserpio, D. M.; Yaghi, O. M. A Porous Covalent Organic Framework with Voided Square Grid Topology for Atmospheric Water Harvesting. *J. Am. Chem. Soc.* **2020**, *142*, 2218−2221.
(25) Banerjee, T.; Haase, F.; Trenker, S.; Biswal, B. P.; Savasci, G.; Duppel, V.; Moudrakovski, I.; Ochsenfeld, C.; Lotsch, B. V. Sub-Stoichiometric 2D Covalent Organic Frameworks from Tri- and Tetratopic Linkers. *Nat. Commun.* **2019**, *10*, 2689.
(26) Karak, S.; Kandambeth, S.; Biswal, B. P.; Sasmal, H. S.; Kumar, S.; Pachfule, P.; Banerjee, R. Constructing Ultraporous Covalent Organic Frameworks in Seconds via an Organic Terracotta Process. *J. Am. Chem. Soc.* **2017**, *139*, 1856−1862.
(27) Biswal, B. P.; Kandambeth, S.; Chandra, S.; Shinde, D. B.; Bera, S.; Karak, S.; Garai, B.; Kharul, U. K.; Banerjee, R. Pore Surface Engineering in Porous, Chemically Stable Covalent Organic Frameworks for Water Adsorption. *J. Mater. Chem. A* **2015**, *3*, 23664−23669.

https://doi.org/10.1021/acscentsci.2c00398
ACS Cent. Sci. 2022, 8, 926−932